Nanoscale

Electronic transport in quantum-dot-in-perovskite solids

Journal:	*Nanoscale*
Manuscript ID	NR-ART-08-2022-004244.R1
Article Type:	Paper
Date Submitted by the Author:	19-Oct-2022
Complete List of Authors:	Erwin, Steven; US Naval Research Laboratory, Center for Computational Materials Science Efros, Alexander; US Naval Research Laboratory, Center for Computational Materials Science

Electronic transport in quantum-dot-in-perovskite solids†

Steven C. Erwin and Alexander L. Efros

Center for Computational Materials Science,

Naval Research Laboratory, Washington, DC 20375

(Dated: October 19, 2022)

Abstract

We investigate theoretically the band transport of electrons and holes in a "quantum-dot-in-perovskite" solid, a periodic array of semiconductor nanocrystal quantum dots embedded in a matrix of lead halide perovskite. For concreteness we focus on PbS quantum dots passivated by inorganic halogen ligands and embedded in a matrix of $CsPbI_3$. We find that the halogen ligands play a decisive role in determining the band offset between the dot and matrix and may therefore provide a straightforward way to control transport experimentally. The model and analysis developed here may readily be generalized to analyze band transport in a broader class of dot-in-solid materials.

The technology for creating nanocrystals by chemical synthesis has improved dramatically over the last 40 years [1]. One feature has nevertheless remained from the earliest days: most nanocrystals are still in some sense embedded in another material—glasses [2] or colloidal solutions [3] or organic ligands [4], for example. The electronic band gap of most matrix materials is generally large and so the embedding does not affect the optical properties of the nanocrystals. But for electronic and optoelectronic device applications, the large band gaps can lead to large band offsets which reduce the tunneling rate and mobility of the carriers and consequently degrade the performance of the device. Moreover, structural and chemical disorder in the matrix may increase the scattering of carriers. Some of these issues have recently been resolved and prototype electronic and optoelectronic devices based on nanocrystal quantum dots have been created—most notably light-emitting diodes [5] and electrically pumped displays [6] and lasers [7].

Nothwithstanding these successes, the broader goal of controlling or even eliminating the deleterious effects of large band offsets and disorder from the matrix remains unrealized. One promising approach is to embed the quantum dots in a *crystalline* matrix. This idea can be traced back to very early work by Itoh on nanocrystals of CuCl grown in a matrix of NaCl [8]. Of course, this particular matrix, although crystalline, has a very large band gap and is therefore still unsuitable for optoelectronic applications.

Another class of crystalline materials—the halide perovskites—are much more attractive as matrix materials for quantum dot electronics because their band gaps are only of order 2–3 eV and can be readily tuned using standard techniques. They also offer the possibility of

embedding quantum dots such as PbS and PbSe *epitaxially* due to a close lattice match with some of the lead halide perovskites. Sargent *et al.* have demonstrated such a quantum-dot-in-perovskite heterocrystal by embedding PbS quantum dots in a matrix of methylammonium lead iodide perovskite, $MAPbI_3$ [9]. They showed that this complex material maintains nearly crystalline order over many dots and attributed to this atomic-scale coherence the excellent optoelectronic properties they observed. Subsequent experimental and theoretical investigation explored how the dot size, surface chemistry, and growth methods affect the resulting optoelectronic properties of this material [10]. Reference [11] discusses recent experimental developments and future prospects for dot-in-perovskites.

Here we develop and analyze a theoretical model of electronic transport in epitaxially coherent quantum-dot-in-perovskite heterocrystals. The model is a periodic generalization of the finite square well model. We determined the parameters of the model using density-functional theory, focusing for concreteness on the material pioneered by Sargent *et al.* of PbS quantum dots but using the slightly simpler inorganic perovskite cesium lead iodide, $CsPbI_3$, which is electronically analogous to $MAPbI_3$. There are two major reasons for choosing this specific pair of materials. First, among the lead halide perovskites the iodide compound has the smallest band gap and therefore the smallest band offset for both types of carriers, a clear benefit for transport via both channels. Second, the crystal structures of $MAPbI_3$ and PbS are closely related and reasonably well lattice-matched, an advantage for creating epitaxially aligned and crystallographically coherent material. In principle, even better lattice matching may be obtainable from the mixed-halide perovskite $MAPb(I,Br)_3$, although a wide miscibility gap may make this goal challenging to reach in practice [12].

We assumed that electron transport is controlled by the overlap of their wavefunctions. There is abundant evidence for band-like conduction in many nanocrystal solids [13–15] although this mechanism is certainly not universal: data from other nanocrystal solids instead exhibit hopping transport [16–19]. However, the overlap of quantum-confined wavefunctions controls transport in both of these limits. We derived an analytic expression for the band width arising from this overlap. This expression reveals how transport depends on the physical dimensions and electronic properties of the dot-in-matrix and reveals the decisive role played by ligands adsorbed on the quantum dots. Our findings should therefore be relevant to a broad range of dot-in-matrix materials.

For optoelectronic technologies based on transport of electrons and holes, the type of

alignment formed by the band gaps of the dot and matrix is a critical consideration. For example, Type I alignment (straddling gaps) would be beneficial for light-emitting diodes, while Type II alignment (staggered gaps) could be advantageous for photovoltaic applications because it results in the rapid separation of carriers. For the electrically pumped devices mentioned earlier—light-emitting diodes [5], displays [6] and lasers [7]—the best performance was achieved when the mobilities of electrons and holes were comparable. The reason for this is simple: the average number of electrons and holes in each dot should be approximately equal. If this neutrality condition is not satisfied, the extra electron or hole can lead to efficient non-radiative Auger recombination that reduces the emission of photons [20]. In this work we therefore assume that Type I alignment with equal valence and conduction band offsets is optimal, but note that this assumption ultimately rests on the particular application one has in mind.

It is well known that the band alignment of colloidal quantum dots depends sensitively on their surface chemistry [21, 22]. Organic molecular ligands adsorbed on the surface, if they have an electric dipole moment, can strongly affect the absolute energy levels of the dot and thus the band alignment relative to the matrix [23]. Organic ligands are not generally employed for dot-in-matrix materials but smaller inorganic ligands are [11]. In particular, halide ions and small halide molecules are frequently used to passivate PbS and PbSe quantun dots because they improve their optical properties [24–26]. Here we show that even a fractional layer of simple *atomic* ligands—that is, individual atoms—adsorbed on the surface can induce a large dipole moment by transferring charge and thus shift the energy levels of the dot by 1 eV or more. We investigate here the example of halogen atoms and demonstrate that by varying their coverage, one can control the band alignment of the dot and matrix and even switch the band alignment from Type I to II, if desired. The ability to control band alignment—and thereby the band transport of electrons and holes—of dot-in-perovskite materials using simple ligand chemistry may help advance these materials further toward their integration into optoelectronic technologies.

I. TECHNICAL APPROACH

We begin with a brief overview of our technical approach. Electron transport in dot-in-perovskite solids has not been widely studied and for this reason the dominant mechanism—

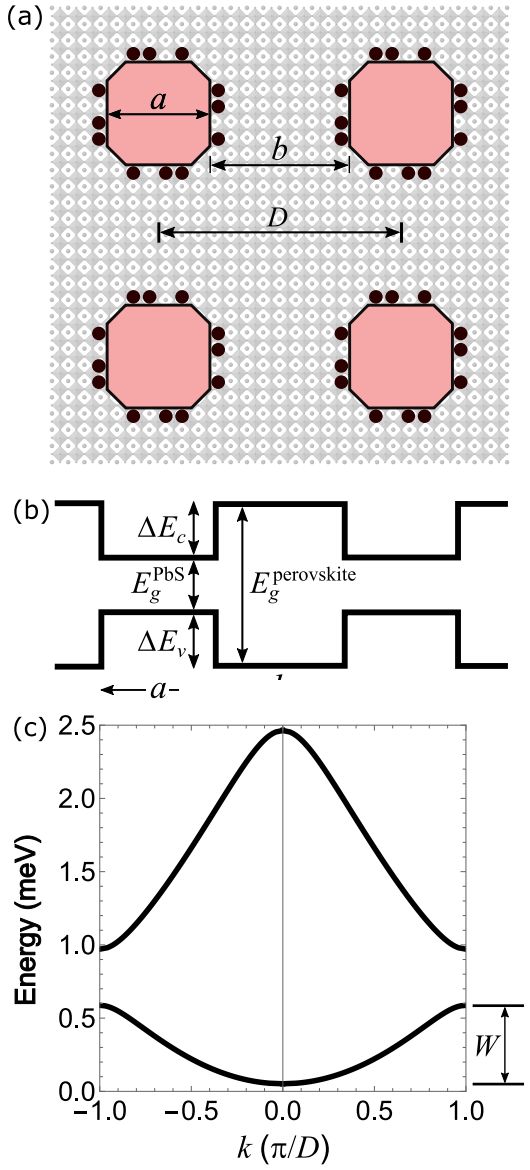

FIG. 1. (a) Three-dimensional cubic lattice of faceted nanocrystal quantum dots embedded in a crystalline matrix of inorganic perovskite. The solid black circles on the nanocrystal surface represent a partial monolayer of metal-atom ligands, for example the halogen atoms discussed in the text. These can be used to tune the band offset between the quantum dots and the perovskite matrix. (b) One-dimensional Kronig-Penney model representing the periodic potential seen by quantum-confined electrons and holes of the dots. The band offsets ΔE_v and ΔE_c depend on the intrinsic offset between the bare dots and the perovskite and are further modified by the electrical dipole created by the metallic ligand layer, as discussed in the text. (c) Lowest two subbands of the Kronig-Penney model. The band width W of the first subband is the central focus of this work.

whether band transport or hopping or something else—is not yet known. Regardless of the mechanism, one of the most critical properties for good transport is the overlap of the quantum-confined wavefunctions of the quantum dots. In previous work we studied this overlap in nanocrystal solids consisting of quantum dots passivated by organic ligands with no embedding matrix [27].

For the dot-in-perovskite sketched in Fig. 1(a) the organic ligands are absent and there is instead a heterointerface between two crystalline materials that includes a layer of halogen ligands (the solid black circles) created intentionally or as part of the quantum dot synthesis [24–26]. We show in Section II that this layer plays a very important and indeed central role in the electronic transport properties. For experimentalists, the choice of the specific ligand and the control of its surface coverage may afford simple yet powerful strategies for controlling transport in dot-in-perovskite materials. There are currently no experimental measurements of the halogen coverage in dot-in-perovskite materials, due to the complications arising from the embedding. However, data for colloidal PbS quantum dots from energy-dispersive X-ray spectroscopy and X-ray photoelectron spectroscopy show coverages consistent with a 1:1 ratio of halogen to surface lead atoms, equivalent to 1 ML coverage [28]. It is therefore plausible that halogen-adsorbed PbS quantum dots could exhibit similar coverages when embedded in perovskite.

Our technical approach is general and can be applied to a wide variety of semiconductor quantum dots embedded in a crystalline matrix. The main idea is illustrated in Fig. 1(b) which represents the three-dimensional solid using a one-dimensional periodic profile for the valence and conduction band edges. This profile defines the well-known Kronig-Penney model [29] for hole and electron states of the dot-in-matrix, respectively.

To apply the Kronig-Penney model to a real material requires accurate values for several important quantities. Some of these are available from experiment, for example the band gaps E_g of the dot and perovskite materials in their bulk crystalline form. Other quantities are not at present available from experiment, for example the valence and conduction band offset between the dot and perovskite bulk materials. We used density-functional theory (DFT) to estimate these as described below.

After determining the numerical values defining the potential profile, we solved the Kronig-Penney model numerically to obtain the energy dispersion $E(k)$ of the electron and hole subbands of the dot-in-perovsite superlattice. A representative example is shown in

Fig. 1(c). For the purpose of characterizing transport we are interested in the band width W of the first, lowest-lying subband, because it quantifies the overlap of the quantum-confined wavefunctions of the dots as they propagate through the surrounding matrix.

In this work we present two types of results for the band width W. In Section II we show numerical results for representative examples of dot size and perovksite width and potential barrier (i.e. the valence or conduction offset). We also derive an analytical expression for W as a function of all the electronic and geometrical parameters defining the material. Our analysis of this expression leads in Section III to several general conclusions about carrier transport in dot-in-matrix materials which may be broadly applied to a wide variety of different material systems.

A. Kronig-Penney model of a periodic square well

The Kronig-Penney model was introduced in 1930 to study the behavior of electrons in the periodic potential arising from the atoms comprising a crystal [29]. The crystal potential was approximated either as a one-dimensional array of square wells representing the atoms or even more simply as delta functions. For modeling the dot-in-perovskite superlattice the use of a square-well potential is especially appropriate because the geometrical and electronic properties of the real material are obviously and directly connected to the shape and height of the square-well potential profile: the diameter a of the quantum dot is the width of the square well and the thickness b of the perovskite matrix is the the width of the barrier region. Likewise the band offsets ΔE_c and ΔE_v are the height of the potential barrier for electrons and holes, respectively.

We will return below to the question of how to determine the potential barriers in the model; here we assume they are given and turn now to obtaining the wave functions and energy band structure of the model. We follow the approach described in Ref. [30] and adopt the same notation. The full solution is in the ESI† (Section S1) and is briefly summarized here.

The wavefunctions in the square well are oscillatory with wavenumber K, while in the barrier they are exponential with wavenumber κ. By applying the usual boundary conditions—that the wavefunction and its derivative (more generally the probability current) are continuous—one obtains an implicit equation for the energy E as a function of the

crystal momentum k,

$$\cos k(a+b) = \mathcal{A}(E), \tag{1}$$

where $\mathcal{A}(E)$ is a complicated oscillatory function of all the parameters in the model given by

$$\cos aK \cosh b\kappa - \sin aK \sinh b\kappa \left(\frac{Km_B}{2\kappa m_W} - \frac{\kappa m_W}{2Km_B} \right). \tag{2}$$

The energy dependence of $\mathcal{A}(E)$ arises from the dispersion relations relating K and κ to the energy E. The simplest choice for these is parabolic dispersion. In Section III and the ESI† (Section S2) we show that the more accurate dispersion afforded by the two-band Kane model does not significantly affect the band width W which is our primary quantity of interest. The effective masses m_W and m_B in the well and barrier, respectively, are constants in the case of parabolic dispersion but depend on energy within the Kane model. In Section S3 of the ESI† we also solve the Kronig-Penney model beyond the effective-mass approximation using the Kane model and find that Eq. 2 indeed still applies.

In practice the Kronig-Penney band structure $E(k)$ is obtained implicitly by choosing a value of k and then numerically solving Eq. 1 for E. Multiple solutions exist for each value of k and correspond to different subbands. The extrema of these subbands occur at $k = 0$ and $k = \pi/(a+b)$ and thus the width W of the lowest subband is given by the difference ΔE between the first roots satisfying $\mathcal{A}(E) = \pm 1$.

B. Dot-in-perovskite structural model

In order to obtain results using the Kronig-Penney model for real materials—here PbS dots and $CsPbI_3$ perovskite—one must determine the barrier heights ΔE_v and ΔE_c as accurately as possible. In this work we used DFT to calculate band offsets for PbS/$CsPbI_3$ isolated interfaces because the methodology is very well established and gives accurate results for many semiconductors including perovskites [31, 32]. In this section we first address an important preliminary question: whether band offsets really can be used for dot-in-perovskite materials, whose geometry is considerably more complicated than an isolated interface.

There are two main complications. First, and most obviously, the surfaces of quantum dots do not in general have a single crystallographic orientation—if they are faceted at all. Using the band offset of a single interface to represent the entire dot-perovskite interface might seem unjustified. However, we can exploit the fact that PbS quantum dots can be

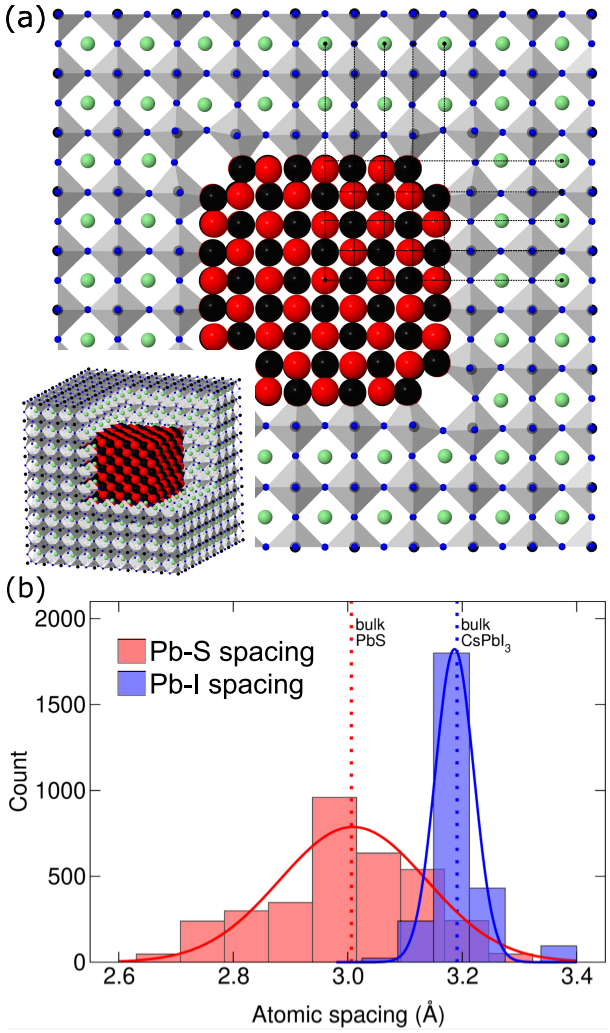

FIG. 2. (a) Fully relaxed dot-in-perovskite consisting of PbS nanocrystal quantum dots embedded in a matrix of $CsPbI_3$ perovskite. The nanocrystals have diameter $a = 2.4$ nm and are almost cubical, with (100) sides and small (110) facets along the edges. The perovskite is assumed to be quasicubic and the terminating surface at the interface is PbI_2. The material is periodic with dot-to-dot spacing $D = 5.1$ nm. The equilibrium geometry shown here was determined from full DFT relaxation. Thin fiducial lines centered on Cs atoms show that the lattice planes in the nanocrystal are approximately 6% closer than in the perovskite, suggesting that each material maintains its own lattice constant despite the interface strain this creates. (b) Histogram of atomic spacings in the nanocrystal (red) and the perovskite (blue). On average, each material maintains its own bulk lattice constant (dotted lines) and therefore the material is best described as unstrained and relaxed.

grown in variety of well-defined shapes, including cubes almost or completely terminated by (100) facets [33]. The band offset between PbS(100) and $CsPbI_3$(100) is therefore likely to reflect with reasonable accuracy the barrier height of the dot-in-matrix. Of course, the true barrier height arises from a finite dot whose edges and corners are not represented by a calculation for an isolated interface. And so it is important to somehow confirm that the true barrier height is close to that of the isolated interface.

The second complication is the strain state of the dot and perovskite. The bulk lattice constants of PbS and $CsPbI_3$ differ by 6%. This difference is small enough to make it likely that the PbS/$CsPbI_3$ interface is atomically coherent with one-to-one atomic registry. For an isolated interface between two infinite materials such registry would necessitate that one or both materials are strained. The exact outcome depends on the elastic constants of the materials. The resulting strain state of the two materials can in general significantly affect the band offset between them [34]. For the dot-in-perovskite the situation is somewhat different: the interface has a finite area and therefore the strain state depends also on this area, the strength of the bonding across the interface, and the volume of the dot. To investigate this complicated situation it is important to understand the true strain state of the dot-in-perovskite material.

We addressed both of these complications by performing a fully relaxed DFT calculation of a realistic dot-in-perovskite crystal, consisting of nearly cubic PbS dots with diameter 2.4 nm and dot-to-dot spacing 5.1 nm. By relaxing the positions of all atoms we obtained detailed information about the strain state of the material at equilibrium. And by analyzing the electrostatic potential $V(\vec{\mathbf{r}})$ of the material we obtained the true barrier height and can directly compare it to the band offset of an isolated interfaces. The detailed results are discussed below in Section II.

C. Density-functional-theory calculations

We used density-functional theory (DFT) with projector-augmented-wave (PAW) potentials, as implemented in VASP [35, 36], to determine the equilibrium structure of the dot-in-perovskite shown in Fig. 2(a) and to estimate band offsets between PbS(100) and $CsPbI_3$(100). The structural relaxations and potential lineup calculations were performed within the generalized-gradient approximation of Perdew, Burke, and Ernzerhof (PBE) [37]

while the bulk band structure calculations used the more accurate hybrid functional of Heyd, Scuseria, and Ernzerhof (HSE) [38]. A supercell for the dot-in-perovskite was defined using the DFT lattice constant for $CsPbI_3$ of 6.38 Å with all atoms initially at ideal lattice sites. The supercell contained a total of 2768 atoms. The positions of all atoms were relaxed until the largest force on any atom was less than 0.07 eV/Å. The relaxed structure is shown in Fig. 2(a). The stress tensor of the supercell was then evaluated using a much larger energy cutoff. The resulting residual pressure was allowed us to estimate the true lattice constant of the relaxed supercell to be only 0.03 Å smaller. This change is negligible compared to the results reported below for the strain state of the dot-in-perovskite and thus the relaxed material may be considered as very close to equilibrium.

The electrostatic potential $V(\vec{\mathbf{r}})$ of the relaxed dot-in-perovskite can be used to obtain the barrier heights for the Kronig-Penney model using the same approach as standard calculations of band offsets (for which a brief summary follows below). The only significant difference is the calculation of the potential alignment between the two materials. For planar interfaces one averages out the atomic-scale variations in $V(\vec{\mathbf{r}})$ by performing a sliding-window average along the direction normal to the interface. For the dot-in-perovskite we instead averaged $V(\vec{\mathbf{r}})$ over individual unit cells containing one formula unit of PbS or $CsPbI_3$ and then performed the potential alignment using the difference of the averaged values near the center of the dot and in the most bulklike part of the perovskite matrix.

We calculated a series of band offsets to investigate how the PbS/$CsPbI_3$ band offset varies when the dot is partially covered by metallic ligand atoms M as shown in Fig. 1(a). We treated this band offset as having two components: 1) the potential alignment between the bare PbS dot in Fig. 2(a) and the $CsPbI_3$ matrix, and 2) the electrostatic shift of PbS(100)-M relative to the bare surface. This approach is in the spirit of "natural" band offsets which have been described in detail elsewhere [31, 39]. We used the PbS(100) surface because that is the dominant facet in our dot-in-perovskite supercell. Four halogen species (F, Cl, Br, I) at varying coverages x in the range 1/8 monolayer (ML) to 1 ML were initially placed atop surface Pb atoms and then relaxed along with the outermost two atomic layers of PbS. An important check of the accuracy of this methodology is to compare the exact offset obtained from the dot-in-perovskite supercell to the natural offset obtained in the case $x = 0$. The agreement is very good as shown in Fig. 3(a) and discussed below.

II. RESULTS

A. Strain state of dot-in-perovskite

For a periodic interface between two nearly lattice-matched materials, the strain state of each material is given by its strain tensor. For the dot-in-perovskite this compact description is not possible and so we turn instead to a statistical description of the strain.

We focus on the nearest-neighbor interatomic distances in the relaxed supercell of Fig. 2(a). Inside the dot these distances correspond to Pb-S atomic spacings whereas inside the perovksite matrix they correspond to Pb-I spacings. A histogram of all the relaxed equilibrium spacings reveals two distinct distributions, both with approximately gaussian form as shown in Fig. 2(b). The Pb-S atomic spacings are centered around a value very close to the theoretical DFT value for bulk PbS (dotted line). Likewise, the Pb-I spacings are sharply peaked around a value very close to the theoretical value for bulk $CsPbI_3$ in its cubic phase.

These distributions establish the important result that the PbS dot and $CsPbI_3$ matrix each maintains, on the average, its own bulk lattice constant. Of course, this situation can only arise if the material creates a varying localized strain field at the dot-perovskite interface. This strain field is indeed evident in the perovskite octahedra at the interfaces in Fig. 2(a) which become increasingly distorted away from the center of the facet. The strain field is also visible from the thin fiducial lines marking the positions of the most bulk-like Cs atoms and revealing a strain field within the Pb-I interfacial bonds at each facet that increases toward the edges of the facet.

In summary, both constituents of the dot-in-perovskite investigated here can be described to a reasonable first approximation as unstrained—with each material at its bulk lattice constant on the average. In light of this we used the DFT bulk lattice constants of PbS and $CsPbI_3$ for the natural band offset calculations described next.

B. Band offset of bare dot-in-perovskite

As discussed above, we used the band offset between PbS(100)-M and $CsPbI_3$(100) to define the barrier heights ΔE_v and ΔE_c of the Kronig-Penney model and we treated the band offset as having two components. In this section we evaluate the accuracy of the first

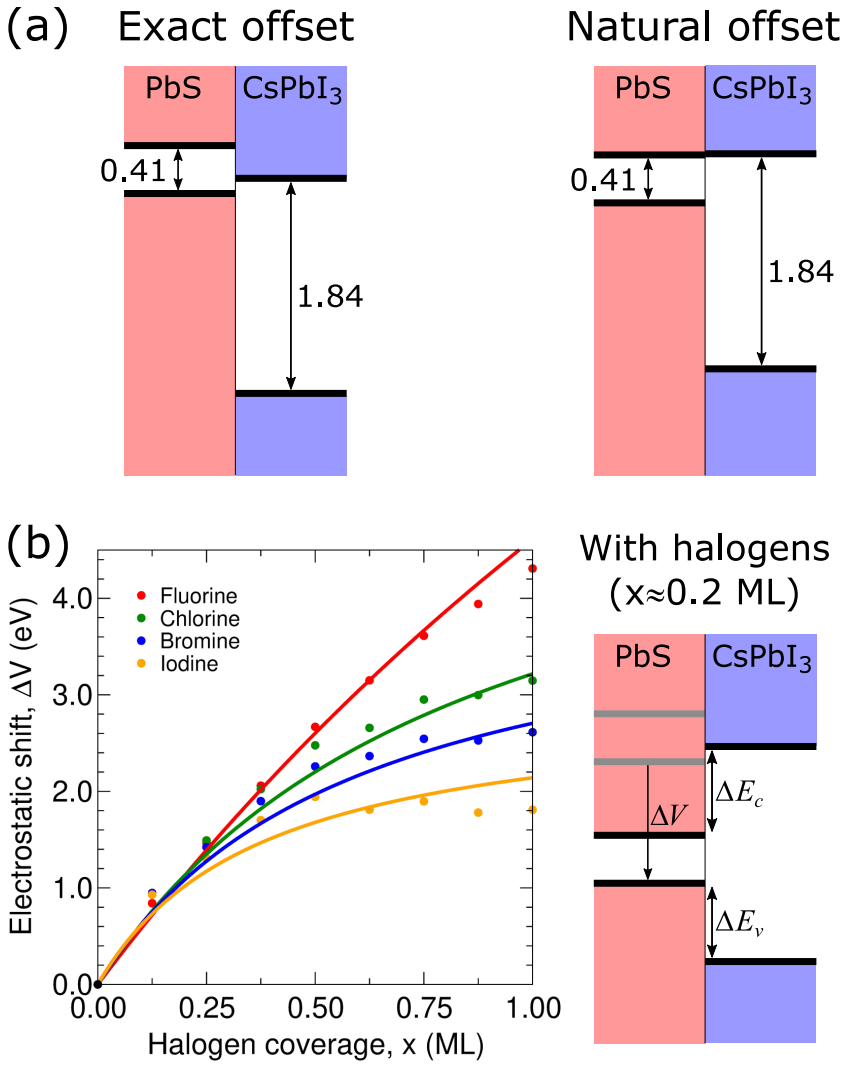

FIG. 3. Theoretical DFT band offsets for the PbS/$CsPbI_3$ dot-in-perovskite. (a) The "exact offset" was determined directly from the calculated alignment of the DFT electrostatic potential for the dot-in-perovskite material shown in Fig. 2(a). The "natural offset" was determined by separately aligning the average electrostatic potentials in thick slabs of PbS(100) and $CsPbI_3$(100) with respect to a common vacuum energy. (b) Theoretical DFT electrostatic shift ΔV of the PbS band edges caused by adsorption of various halogen atom ligands on the PbS(100) surface. At low coverages x all four halogens lead to similar downward shifts. The curves are a two-parameter fit to the DFT values (solid symbols) of the simple electrostatic model proposed in the ESI† (Section S5). The band diagram to the right illustrates the fact that 0.2 ML shifts the bands down by about 1 eV, changing the staggered Type II alignment in panel (a) to Type I alignment with approximately equal valence and conduction band offsets.

component by comparing the band offset obtained from the exact dot-in-perovskite potential to the natural band offset of bare PbS(100) and $CsPbI_3$(100).

There are many reasons why natural band offsets might not accurately represent the exact band offset of the dot-in-perovskite. The former relies on two separate calculations for the free (100) surfaces, while the latter includes a complicated interface with locally strained bonds as well as edges and corners—all of which are neglected in the natural offset approach. To investigate the accuracy of this approach we compare in Fig. 3(a) the exact and natural band offsets in the absence of ligands. The agreement is remarkably good—the exact and natural valence offsets are 1.7 and 1.4 eV, respectively. (For these results and all others reported below, we used DFT to calculate ΔE_v and then added the bulk band gap to obtain ΔE_c.)

This small difference between the exact and natural result arises because the latter omits a subtle effect that occurs at the interface. Consider the layer of Pb and S atoms at the interface with $CsPbI_3$. The Pb atoms are directly across from I atoms and are attracted to them electrostatically and therefore shift toward them (by 0.26 Å). The S atoms are of two types: 3/4 of them are directly across from Pb atoms and similarly shift toward them (by 0.21 Å). But 1/4 of the S atoms are across from Cs atoms that are one lattice plane more distant. These S atoms experience very little attraction and so do not shift. In summary, all of the Pb atoms shift but only 3/4 of S atoms shift and so the surface develops a small dipole moment. The potential discontinuity from this dipole is about 0.4 eV. This subtle effect is included in the exact offset but not in the natural offset.

C. Shift of the band offset by halogen ligands

Armed with the knowledge that natural band offsets accurately reproduce the exact offsets, we now turn to the dramatic effects of the halogen ligands on the band offset of PbS/$CsPbI_3$. We restricted our investigation to partial monolayers of the halogens F, Cl, Br, and I with coverage x between 0 and 1. Halogen atoms are highly electronegative and when adsorbed as ligands they shift electron charge from the PbS surface region toward the halogen layer, creating a dipole layer that pulls down the energies of PbS states. At low halogen coverages x this electrostatic shift ΔV is proportional to x with a similar magnitude for all four halogen species, as shown in Fig. 3(b). For example, a partial halogen layer with

very modest coverage $x = 0.2$ ML shifts the PbS band edges strongly downward by about 1 eV. We apply this shift to the exact offset of the bare dot-in-perovskite and see that it is sufficiently large to change the staggered Type II alignment in Fig. 3(a) to Type I alignment with roughly equal values of ΔE_v and ΔE_c as shown in Fig. 3(b).

At higher halogen coverages the electric field of the dipole layer begins polarize the halogen atoms, which creates an opposing dipole moment [40]. For this reason the electrostatic shift eventually saturates, as shown in Fig. 3(b). The saturated value scales inversely with the atomic polarizability of the halogen atom, as demonstrated in the ESI† (Section S5) using a simple model of the shift. When the monolayer is fully complete, fluorine atoms create a shift about twice as large as iodine atoms whereas chlorine and bromine create intermediate shifts.

In summary, even relatively modest amounts of halogen ligands adsorbed on the PbS quantum dot lead to large changes in the band offset of the dot-in-perovskite: a rough rule of thumb is that every 0.01 ML of halogen atoms shifts the band offset by approximately 70 meV until saturation begins to set in.

D. Band width of dot-in-perovskite

We turn now to our central focus—the band width of the lowest electron and hole subbands for dot-in-perovskite materials. Our goal is two-fold. First, we seek a broad understanding of how the band width changes as a function of the various parameters in the Kronig-Penney model. Second, we will show in Section III how our results can be used to create an experimental strategy for optimizing carrier transport in the specific PbS-M/$CsPbI_3$ dot-in-perovskite material.

The Kronig-Penney model is a periodic array of finite quantum wells. Therefore the overlap of the tails of bound-state wavefunctions should decay approximately exponentially with the square root of the potential barrier height U (which represents ΔE_c in the case of electron states and ΔE_v in the case of hole states). This expectation is confirmed by numerically calculating the Kronig-Penney band width W as a function of U for three typical values of the dot diameter a and a fixed value of the perovskite thickness $b = 4$ nm; see the symbols and thick solid curves in Fig. 4(a). Dispersion relations for the Kane model were used along with experimental values for the material parameters. The calculated

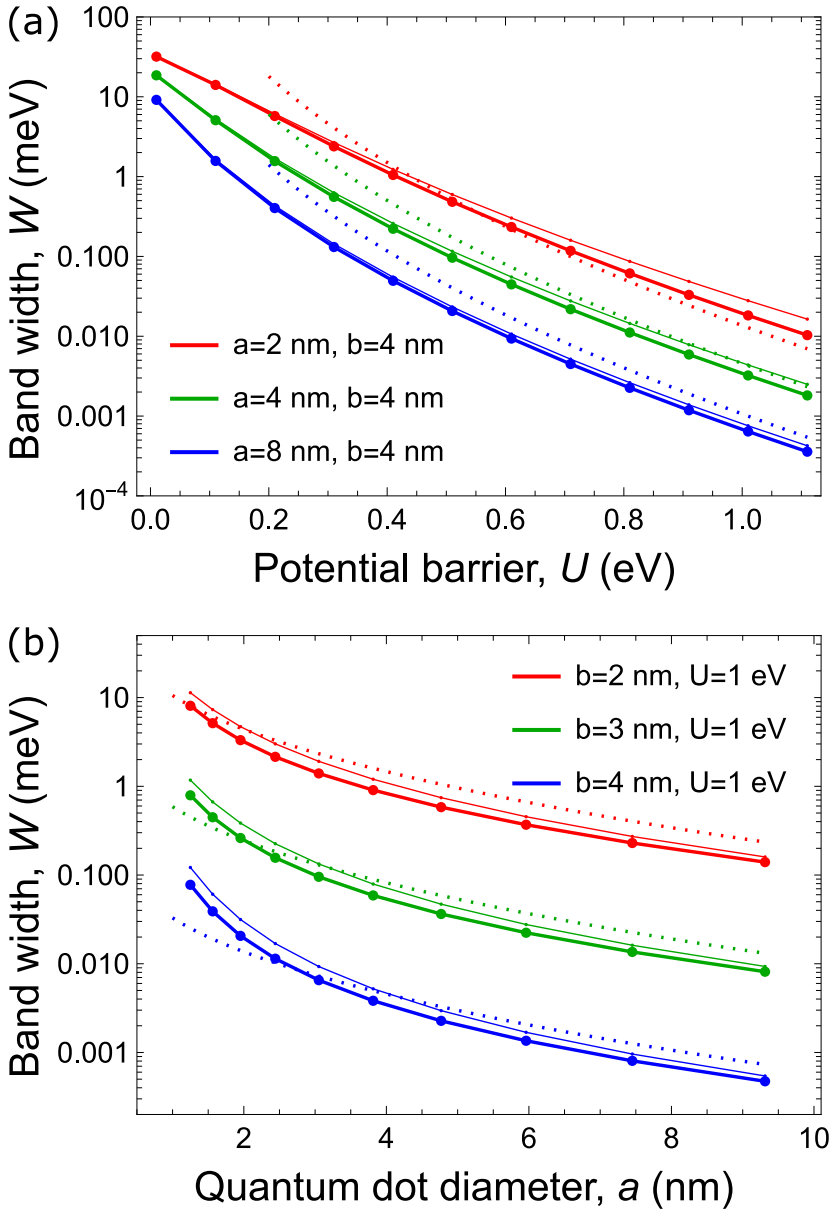

FIG. 4. Theoretical band width W of the first electron and hole subbands of the dot-in-perovskite. (a) Variation of W with the potential barrier U, for the case of constant perovskite thickess $b = 4$ nm separating PbS quantum dots of different diameters. The barrier U corresponds to the band offset ΔE_c or ΔE_v shown in Fig. 3(b). Red, green, and blue curves are for dot diameters $a = 2$, 4, and 8 nm, respectively. (b) Variation of W with the quantum dot diameter a, for a fixed potential barrier $U = 1$ eV. Red, green, and blue curves are for perovskite thicknesses $b = 2$, 3, and 4 nm, respectively. Symbols and thick solid curves are the exact Kronig-Penney band width. Thin solid curves were obtained using parabolic dispersion for comparison. Dotted curves are the approximate analytical expression $\tilde{W}$ discussed in the text.

results show that the band width for very small barrier heights (i.e. for nearly free electron or hole states) is of order 10 meV and falls by roughly four orders of magnitude for barriers around 1 eV.

To understand these numerical results more broadly we have derived an analytical approximation for W valid when the barrier height is sufficiently large. The full derivation is in the ESI† (Section S3) and the result is

$$\tilde{W} = e^{-(U/U_0)^{1/2}} W_0. \tag{3}$$

Here we have defined a characteristic energy associated with the barrier, $U_0 = \hbar^2/2m_B b^2$. This expression is valid when U is large compared to U_0. The prefactor W_0 has the general form

$$W_0 = 4\sqrt{2}\left(\frac{m_B}{m_W}\right)\left(\frac{K}{K'}\right)\left(\frac{\hbar^2/m_B a^2}{U}\right)^{1/2} \tag{4}$$

where the prime denotes the derivative with respect to energy and therefore K/K' has units of energy. If specific dispersion relations are assumed then a more explicit expression can be obtained; see the ESI† (Section S2) for the explicit forms for parabolic dispersion and Kane-model dispersion. In our case U_0 is of order 10 meV and therefore $\tilde{W}$ should be a good approximation to the exact W for most of the range of U shown in Fig. 4(a). This expectation is confirmed by the thin dotted curves, which closely track the exact results except at very small values of U.

We also investigated the sensitivity of the band width to the accuracy of the expressions used to describe the dispersion relations of the materials. For example, the thin solid curves show the exact W obtained using standard parabolic dispersion—which is less accurate but more familiar than the Kane model—for both regions. Their very close similarity to the thick curves establishes that very accurate reproduction of the dispersion is probably not necessary for calculating the band width.

Finally, we turn to the dependence of the band width on the diameter a of the PbS quantum dots. It is a general feature of quantum wells with finite barriers that smaller wells lead to more wavefunction "leakage" into the barrier. One therefore expects that the Kronig-Penney band width should decrease as the size of the quantum dot increases. Indeed by analyzing the behavior of W_0 it is easy to show that for physically relevant sizes the band width scales as $1/a^3$ regardless of the nature of the dispersion. This expectation is confirmed in Fig. 4(b) which shows results for three values of the perovskite thickness and

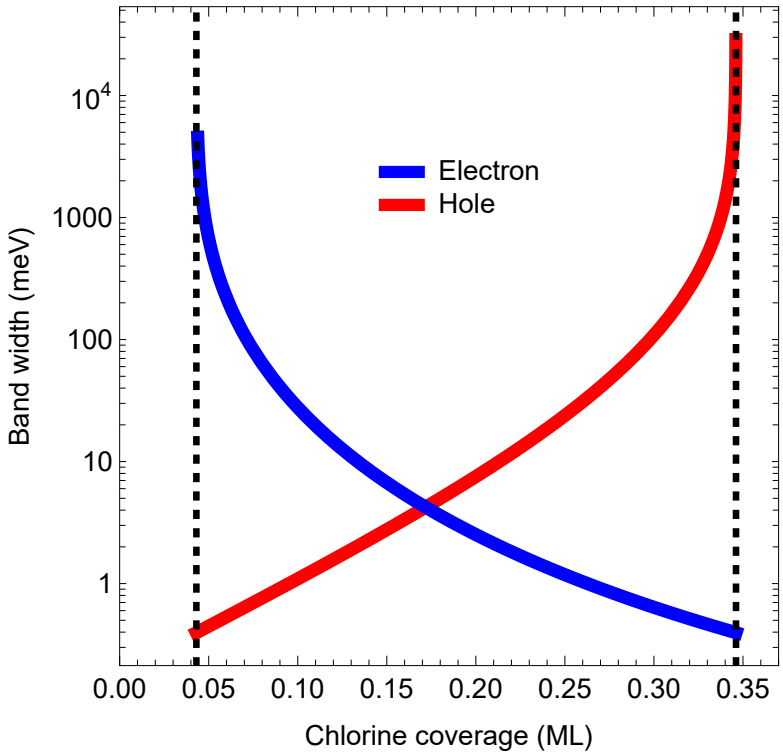

FIG. 5. Theoretical band width of the electron and hole subbands of the dot-in-perovskite as a function of the coverage of halogen atoms adsorbed on the quantum dots. The dashed black lines show the minimum and maximum coverage values that lead to quantum confinement within the dot for both electron and hole states. The band widths shown are for chlorine halogens, with PbS dot diameter $a = 4$ nm and $CsPbI_3$ perovskite thickness $b = 2$ nm, but other halogens and physical sizes lead to qualitatively similar results.

a fixed value of the potential barrier $U = 1$ eV. The calculated results show that in this size range, changing the dot size by a factor two changes the band width by roughly one order of magnitude. This effect may therefore be an important consideration in the design of transport experiments.

III. DISCUSSION

We now bring together the results of the previous section—for the strain state, the band offsets, the halogen ligands, and the band width—to answer the question, how can one experimentally optimize carrier transport in dot-in-perovskite materials? As discussed in

the introduction, we use the term "optimize" here in the sense of balancing the transport in the electron and hole channels to make them comparable.

The idea is very simple and is illustrated in Fig. 5. We use the example of chlorine ligands but the result for other halogens is very similar. Recall that without any ligands, the dot-in-perovskite band offset has staggered Type II alignment as shown in Fig. 3(a). A very small chlorine coverage of 0.04 ML is sufficient to change this alignment to Type I. This borderline situation leads to nearly free electron states but maximally confined holes states. At higher coverages around 0.35 ML the situation is the opposite: nearly free hole states and maximally confined electron states. Figure 5 shows that an intermediate coverage of 0.17 ML is optimal in the sense that the band widths for electron and holes states are then equal.

At such low values of the ligand coverage all four halogens lead to very similar electrostatic shifts, because the electric field is relatively small and therefore saturation has not yet set in. The optimal coverage for fluorine, bromine, and iodine should therefore be nearly the same as for chlorine.

We close by briefly discussing several issues that may warrant revisiting in future work. For simplicity we have used here the cubic phase of $CsPbI_3$ but in reality this phase is stable only at high temperature [41]. The stable phase at room temperature is distorted and possibly has a polymorphous crystal structure [42]. Including such effects in our modeling would not be difficult but we believe the results would not be very much affected. Likewise we have kept our model simple by considering PbS dots having a shape close to cubes. More complicated shapes with several different crystallographic facets would complicate the model but would not change the basic approach. Another interesting issue concerns the interface between PbS and $CsPbI_3$, which we assumed to be at the PbI_2-terminated (100) plane of the perovskite because this makes sense chemically and electrostatically. However, this assumption may not survive in the presence of the ligands or, more obviously, for other crystallographic facets. Due to the ionic nature of perovskites, differently terminated interfaces can in principle lead to very large changes in the band offset (of order 1 to 2 eV) with profound consequences for transport properties. This issue is difficult to investigate both theoretically and experimentally but it may be important.

IV. CONCLUSIONS

We developed a theoretical Kronig-Penney model for the band transport of electrons and holes in a quantum-dot-in-perovskite solid, focusing for concreteness on PbS quantum dots passivated by inorganic halogen ligands and embedded in a matrix of $CsPbI_3$. This model yields materials-specific results for the band width of the lowest-lying electron and hole subbands. The results reveal the central role played by the ligands, which create an electrostatic shift of the band edges that can easily exceed 1 eV and thereby switch the band offset from its native Type II alignment to Type I alignment, which is required for optoelectronic applications.

Although we focused on PbS quantum dots in $CsPbI_3$, our model and analysis may be easily generalized to analyze band transport in a broader class of dot-in-solid materials. Toward this goal, we also derived an analytical expression for the Kronig-Penney band width that reveals its detailed dependence on the physical geometry of the dot-in-matrix as well as the electronic characteristics of the materials. We anticipate that this expression will aid the development and refinement of new dot-in-matrix materials with improved transport properties.

V. CONFLICTS OF INTEREST

There are no conflicts of interest to declare.

VI. ACKNOWLEDGMENTS

This work was supported by the Office of Naval Research through Award N0001418WX01839 and through the Naval Research Laboratory's Basic Research Program.

†Electronic supplementary information (ESI) available: Kronig-Penney model in the effective-mass approximation; Analytical expression for the width of the lowest subband of the Kronig-Penney model; Kronig-Penney model beyond the effective-mass approximation: Kane model of coupled valence and conduction bands; Material parameters for the Kronig-Penney model; Simple model of the electrostatic shift from the halogen ligands. See DOI:

10.1039/ 0000000000

[1] Al. L. Efros and L. E. Brus, Nanocrystal quantum dots: From discovery to modern development, ACS Nano **15**, 6192 (2021).

[2] A. I. Ekimov and A. A. Onushchenko, Quantum size effect in three-dimensional microscopic semiconductor crystals, JETP Lett. **34**, 6345 (1981).

[3] L. E. Brus, A simple model for the ionization potential, electron affinity, and aqueous redox potentials of small semiconductor crystallites, J. Chem. Phys. **79**, 5566 (1983).

[4] C. B. Murray, D. J. Norris, and M. G. Bawendi, Synthesis and characterization of nearly monodisperse CdE (E = S, Se, Te) semiconductor nanocrystallites, Journal of the American Chemical Society **115**, 8706 (1993).

[5] J. Kim, D. Hahm, W. K. Bae, H. Lee, and J. Kwak, Transient dynamics of charges and excitons in quantum dot light-emitting diodes, Small **18**, 2202290 (2022).

[6] Y. H. Won, O. Cho, T. Kim, D. Y. Chung, T. Kim, H. Chung, H. Jang, J. Lee, D. Kim, and E. Jang, Highly efficient and stable InP/ZnSe/ZnS quantum dot light-emitting diodes, Nature **575**, 634 (2019).

[7] H. Jung, N. Ahn, and V. I. Klimov, Prospects and challenges of colloidal quantum dot laser diodes, Nature Photonics **15**, 643 (2021).

[8] T. Itoh and T. Kirihara, Excitons in CuC1 microcrystals embedded in NaCl, Journal of Luminescence **32**, 120 (1984).

[9] Z. Ning, X. Gong, R. Comin, G. Walters, F. Fan, O. Voznyy, E. Yassitepe, A. Buin, S. Hoogland, and E. H. Sargent, Quantum-dot-in-perovskite solids, Nature **523**, 324 (2015).

[10] E. A. Gaulding, X. Chen, Y. Yang, S. P. Harvey, B. To, Y. H. Kim, M. C. Beard, P. C. Sercel, and J. M. Luther, Embedding PbS quantum dots (QDs) in Pb-halide perovskite matrices: QD surface chemistry and antisolvent effects on QD dispersion and confinement properties, ACS Materials Letters **2**, 1464 (2020).

[11] H. Chen, J. M. Pina, Y. Hou, and E. H. Sargent, Synthesis, applications, and prospects of quantum-dot-in-perovskite solids, Advanced Energy Materials **12** (2022).

[12] F. Lehmann, A. Franz, D. M. Többens, S. Levcenco, T. Unold, A. Taubert, and S. Schorr, The phase diagram of a mixed halide (Br, I) hybrid perovskite obtained by synchrotron X-ray

diffraction, RSC Advances **9**, 11151 (2019).

[13] E. Talgorn, Y. Gao, M. Aerts, L. T. Kunneman, J. M. Schins, T. J. Savenije, M. A. Van Huis, H. S. Van Der Zant, A. J. Houtepen, and L. D. Siebbeles, Unity quantum yield of photogenerated charges and band-like transport in quantum-dot solids, Nature Nanotechnology **6**, 733 (2011).

[14] Y. Liu, N. Peard, and J. C. Grossman, Bandlike Transport in PbS Quantum Dot Superlattices with Quantum Confinement, Journal of Physical Chemistry Letters **10**, 3756 (2019).

[15] X. Lan, M. Chen, M. H. Hudson, V. Kamysbayev, Y. Wang, P. Guyot-Sionnest, and D. V. Talapin, Quantum dot solids showing state-resolved band-like transport, Nature Materials **19**, 323 (2020).

[16] Y. Liu, M. Gibbs, J. Puthussery, S. Gaik, R. Ihly, H. W. Hillhouse, and M. Law, Dependence of carrier mobility on nanocrystal size and ligand length in pbse nanocrystal solids, Nano Letters **10**, 1960 (2010).

[17] P. Guyot-Sionnest, Electrical transport in colloidal quantum dot films, Journal of Physical Chemistry Letters **3**, 1169 (2012).

[18] K. Whitham, J. Yang, B. H. Savitzky, L. F. Kourkoutis, F. Wise, and T. Hanrath, Charge transport and localization in atomically coherent quantum dot solids, Nature Materials **15**, 557 (2016).

[19] R. H. Gilmore, S. W. Winslow, E. M. Lee, M. N. Ashner, K. G. Yager, A. P. Willard, and W. A. Tisdale, Inverse temperature dependence of charge carrier hopping in quantum dot solids, ACS Nano **12**, 7741 (2018).

[20] Al. L. Efros and D. J. Nesbitt, Origin and control of blinking in quantum dots, Nature Nanotechnology **11**, 661 (2016).

[21] B. A. Timp and X. Y. Zhu, Electronic energy alignment at the PbSe quantum dots/ZnO(1010) interface, Surface Science **604**, 1335 (2010).

[22] W. M. Lin, M. Yarema, M. Liu, E. Sargent, and V. Wood, Nanocrystal quantum dot devices: How the lead sulfide (PbS) system teaches us the importance of surfaces, Chimia **75**, 398 (2021).

[23] P. R. Brown, D. Kim, R. R. Lunt, N. Zhao, M. G. Bawendi, J. C. Grossman, and V. Bulović, Energy level modification in lead sulfide quantum dot thin films through ligand exchange, ACS Nano **8**, 5863 (2014).

[24] W. K. Bae, J. Joo, L. A. Padilha, J. Won, D. C. Lee, Q. Lin, W. K. Koh, H. Luo, V. I. Klimov, and J. M. Pietryga, Highly effective surface passivation of PbSe quantum dots through reaction with molecular chlorine, Journal of the American Chemical Society **134**, 20160 (2012).

[25] J. Zhang, J. Gao, E. M. Miller, J. M. Luther, and M. C. Beard, Diffusion-controlled synthesis of PbS and PbSe quantum dots with in situ halide passivation for quantum dot solar cells, ACS Nano **8**, 614 (2014).

[26] R. W. Crisp, D. M. Kroupa, A. R. Marshall, E. M. Miller, J. Zhang, M. C. Beard, and J. M. Luther, Metal halide solid-state surface treatment for high efficiency PbS and PbSe QD solar cells, Scientific Reports **5** (2015).

[27] A. R. Khabibullin, Al. L. Efros, and S. C. Erwin, The role of ligands in electron transport in nanocrystal solids, Nanoscale **12**, 23028 (2020).

[28] J. Tang, K. W. Kemp, S. Hoogland, K. S. Jeong, H. Liu, L. Levina, M. Furukawa, X. Wang, R. Debnath, D. Cha, K. W. Chou, A. Fischer, A. Amassian, J. B. Asbury, and E. H. Sargent, Colloidal-quantum-dot photovoltaics using atomic-ligand passivation, Nature Materials **10**, 765 (2011).

[29] R. de L. Kronig and W. G. Penney, Quantum mechanics of electrons in crystal lattices, Proceedings of the Royal Society A: Mathematical, Physical and Engineering Sciences **130**, 499 (1931).

[30] M. Grundmann, *The Physics of Semiconductors: An Introduction Including Devices and Nanophysics* (Springer, 2010).

[31] L. Weston, H. Tailor, K. Krishnaswamy, L. Bjaalie, and C. G. Van de Walle, Accurate and efficient band-offset calculations from density functional theory, Computational Materials Science **151**, 174 (2018).

[32] J. L. Lyons, Effective donor dopants for lead halide perovskites, Chemistry of Materials **33**, 6200 (2021).

[33] Y. Jiang, Y. Wu, B. Xie, S. Yuan, X. Liu, and Y. Qian, Hydrothermal preparation of uniform cubic-shaped PbS nanocrystals, Journal of Crystal Growth **231**, 248 (2001).

[34] C. G. Van de Walle, Band lineups and deformation potentials in the model-solid theory, Physical Review B **39**, 1871 (1989).

[35] G. Kresse and J. Furthmüller, Efficiency of ab-initio total energy calculations for metals and semiconductors using a plane-wave basis set, Physical Review B **6**, 15 (1996).

[36] P. E. Blöchl, Projector augmented-wave method, Physical Review B **50**, 17953 (1994).

[37] J. P. Perdew, K. Burke, and M. Ernzerhof, Generalized Gradient Approximation Made Simple, Physical Review Letters **77**, 3865 (1996).

[38] J. Heyd, G. E. Scuseria, and M. Ernzerhof, Hybrid functionals based on a screened coulomb potential, The Journal of Chemical Physics **118**, 8207 (2003).

[39] W. A. Harrison, *Electronic Structure and the Properties of Solids* (Freeman, 1980).

[40] F. Gossenberger, T. Roman, K. Forster-Tonigold, and A. Groß, Change of the work function of platinum electrodes induced by halide adsorption, Beilstein Journal of Nanotechnology **5**, 152 (2014).

[41] C. C. Stoumpos, C. D. Malliakas, and M. G. Kanatzidis, Semiconducting tin and lead iodide perovskites with organic cations: Phase transitions, high mobilities, and near-infrared photoluminescent properties, Inorganic Chemistry **52**, 9019 (2013).

[42] X. G. Zhao, Z. Wang, O. I. Malyi, and A. Zunger, Effect of static local distortions vs. dynamic motions on the stability and band gaps of cubic oxide and halide perovskites, Materials Today **49**, 107 (2021).